Journal of Magnetism and Magnetic Materials ∎ (∎∎∎∎) ∎∎∎–∎∎∎

Contents lists available at ScienceDirect

Journal of Magnetism and Magnetic Materials

journal homepage: www.elsevier.com/locate/jmmm

Single crystal study of layered U_nRhIn_{3n+2} materials: Case of the novel U_2RhIn_8 compound

Attila Bartha [a,*], M. Kratochvílová [a], M. Dušek [b], M. Diviš [a], J. Custers [a], V. Sechovský [a]

[a] Department of Condensed Matter Physics, Charles University, Ke Karlovu 5, 121 16 Praha 2, Czech Republic
[b] Department of Structure Analysis, Institute of Physics ASCR, Cukrovarnická 10, 162 00 Praha 6, Czech Republic

ARTICLE INFO

Article history:
Received 17 November 2014
Received in revised form
8 January 2015
Accepted 8 January 2015

Keywords:
Single crystal growth
Antiferromagnetism
Magnetocrystalline anisotropy
U_2RhIn_8

ABSTRACT

We report on the single crystal properties of the novel U_2RhIn_8 compound studied in the context of parent $URhIn_5$ and UIn_3 systems. The compounds were prepared by In self-flux method. U_2RhIn_8 adopts the Ho_2CoGa_8-type structure with lattice parameters $a=4.6056(6)$ Å and $c=11.9911(15)$ Å. The behavior of U_2RhIn_8 strongly resembles that of the related $URhIn_5$ and UIn_3 with respect to magnetization, specific heat and resistivity except for magnetocrystalline anisotropy developing with lowering dimensionality in the series UIn_3 vs. U_2RhIn_8 and $URhIn_5$. U_2RhIn_8 orders antiferromagnetically below $T_N=117$ K and exhibits a slightly enhanced Sommerfeld coefficient $\gamma=47$ mJ mol^{-1} K^{-2}. Magnetic field leaves the value of Néel temperature for both $URhIn_5$ and U_2RhIn_8 unaffected up to 9 T. On the other hand, T_N is increasing when applying hydrostatic pressure up to 3.2 GPa. The character of uranium 5*f* electron states of U_2RhIn_8 was studied by first principles calculations based on the density functional theory. The overall phase diagram of U_2RhIn_8 is discussed in the context of magnetism in the related $URhX_5$ and UX_3 (X=In, Ga) compounds.

© 2015 Published by Elsevier B.V.

UNCORRECTED PROOF

1. Introduction

Magnetism of uranium compounds is characterized by the large spatial extent of the 5*f* wave functions which perceive their physical surroundings more intensively compared to the localized behavior of 4*f* electrons. Typical example of that is the 5*f*-ligand hybridization causing nonmagnetic behavior in several compounds characterized by the distance between the nearest U ions far larger than the Hill limit [1]. When considering the UX_3 (X=*p*-metal) materials, the size of the *p*-atom is a very important parameter. In the case of smaller *X*-ions (Si, Ge) [2], the *p*-wave function decays slower at the U-site, resulting in strong 5*f*–*p* hybridization which leads to lack of magnetic ordering (UGe_3, USi_3) [4,2,3] while larger *X*-ions (In, Pb) cause the hybridization to be weaker resulting in magnetic ground state (UIn_3, UPb_3) [5,6].

The U_nTX_{3n+2} (n=1, 2; T=transition metal; X= In, Ga) [7–9,19,24] compounds adopt the layered Ho_nCoGa_{3n+2}-type structure which consists of n UX_3 layers alternating with a TX_2 layer sequentially along the [001] direction in the tetragonal lattice. They are isostructural with the thoroughly investigated Ce_nTX_{3n+2} [10] compounds known for their outstanding physical properties such as the coexistence of unconventional superconductivity and magnetism or non-Fermi liquid behavior. These families of compounds provide unique opportunity to study the effect of dimensionality on physical properties due to their layered tetragonal structure. Adding a layer of TX_2 pushes the character of the structural dimensionality from 3D to more 2D.

Since the U_2RhIn_8 compound has not been reported yet, we focused in this paper on the structure study followed by investigation of magnetic, transport and thermodynamic properties with respect to applied magnetic fields and hydrostatic pressure. In order to study the evolution of ground state properties on the structural dimensionality, we also prepared and investigated single crystals of $URhIn_5$ and UIn_3.

2. Experimental

Single crystals of UIn_3, $URhIn_5$ and U_2RhIn_8 have been prepared using In self-flux method. High-quality elements U (purified by SSE [11]), Rh (3N5) and In (5N) were used. The starting composition of U:In=1:10, U:Rh:In=1:1:25 and U:Rh:In=2:1:25 was placed in alumina crucibles in order to obtain UIn_3, $URhIn_5$ and U_2RhIn_8, respectively. The crucibles were further sealed in evacuated quartz tubes. The ampoules were then heated up to 950 °C, kept at this temperature for 10 h to let the mixture homogenize properly and consequently cooled down to 600 °C in 120 h. After decanting, plate-like single crystals of U_2RhIn_8 ($URhIn_5$) with

* Corresponding author. Tel.: +420 221911456.
E-mail address: bartha@mag.mff.cuni.cz (A. Bartha).

http://dx.doi.org/10.1016/j.jmmm.2015.01.015
0304-8853/© 2015 Published by Elsevier B.V.

typical dimensions of $1 \times 0.5 \times 0.3$ mm^3 ($1 \times 1 \times 0.5$ mm^3) were obtained. In case of UIn_3, however, our attempts led to growth of single crystals of typical masses <0.1 mg. The single crystal of UIn_3 ($2 \times 2 \times 2$ mm^3) suitable for the bulk measurements was obtained as a by-product of the $URhIn_5$ synthesis.

Homogeneity and chemical composition of the single crystals were confirmed by scanning electron microscope (Tescan MIRA I LMH SEM) equipped with energy dispersive *X*-ray analyzer (Bruker AXS). The crystal structures were determined by single crystal *X*-ray diffraction using *X*-ray diffractometer Gemini, equipped with an Mo lamp, graphite monochromator and an Mo-enhance collimator producing Mo K_α radiation, and a CCD detector Atlas. Absorption correction of the strongly absorbing samples ($\mu \sim 50$ mm^{-1}) was done by the combination of the numerical absorption correction based on the crystal shapes and empirical absorption correction based on spherical harmonic functions, using the software of the diffractometer CrysAlis PRO. The crystal structures were solved by SUPERFLIP [13] and refined by software Jana2006 [14].

The electrical resistivity measurements were done utilizing the standard four-point method down to 2 K in a Physical Property Measurement System (PPMS). The specific heat measurements down to 400 mK were carried out using the He3 option. Magnetization measurements were performed in a superconducting quantum interference device (MPMS) from 2 to 300 K/400 K and magnetic fields up to 7 T.

To investigate the effect of hydrostatic pressure on the transition temperature T_N, we measured the temperature dependence of electrical resistivity using a double-layered (CuBe/NiCrAl) piston-cylinder type pressure cell with Daphne 7373 oil as the pressure-transmitting medium [15,16]. Pressures up to 3.2 GPa were reached.

In order to acquire information about formation of magnetic moments in U_2RhIn_8, we applied the theoretical methods based on the density functional theory. The electronic structure and magnetic moments were calculated using the latest version of APW+lo WIEN2k code [17]. The 5*f* electrons form the Bloch states with non-integer occupation number. The spin–orbit coupling was included using second-order variational step [18]. Since we found the smaller value of the total magnetic moment than expected, we applied the LSDA+U method [17] and tuned the effective U to obtain the required total magnetic moment. The electronic structure calculations were performed at experimental equilibrium. The calculations were ferromagnetic for the sake of simplicity, since we have no information about the character of the antiferromagnetic ground state.

3. Results and discussion

The obtained diffraction patterns revealed the Ho_2CoGa_8-($HoCoGa_5$)-type structure (P4/mmm) for U_2RhIn_8 ($URhIn_5$). Table 1 summarizes the lattice parameters, atomic coordinates and the equivalent isotropic displacement parameters U_{eq}. The refinement parameters of the obtained data for U_2RhIn_8 equal $R_{int} = 0.076$, $R[F^2 > 3\sigma F^2] = 0.035$, the largest peak/hole in difference Fourier map $\Delta\rho_{max} = 5.84$ eÅ^{-3}/$\Delta\rho_{min} = -4.04$ eÅ^{-3}. For $URhIn_5$: $R_{int} = 0.041$, $R[F^2 > 3\sigma F^2] = 0.022$, $\Delta\rho_{max} = 2.55$ eÅ^{-3}/$\Delta\rho_{min} = -2.01$ eÅ^{-3}.

The temperature dependence of the specific heat $C(T)$ divided by temperature for U_2RhIn_8 and $URhIn_5$ is presented in Fig. 1; a clear λ-shaped anomaly at $T_N = 117$ K and $T_N = 98$ K, respectively, indicates a second-order phase transition in both materials. Closer observation of the $C(T)$ vs. T curve of U_2RhIn_8 reveals a small anomaly at $T \sim 100$ K, which arises from a tiny amount of $URhIn_5$.

Table 1
Lattice parameters, fractional atomic coordinates and isotropic or equivalent isotropic displacement parameters for U_2RhIn_8 and $URhIn_5$.

	Atom	*x*	*y*	*z*	U^*_{iso}/U_{eq}
U_2RhIn_8					
$a = 4.6056(6)$ Å	U	0.5	0.5	0.30883(7)	0.0059(3)
$c = 11.9911(15)$ Å	Rh	0.5	−0.5	0	0.0078(6)
	In(1)	0.5	0	0.5	0.0080(5)
	In(2)	0.5	0	0.12263(11)	0.0091(4)
	In(3)	0	0	0.30916(14)	0.0079(4)
$a = 4.6210(5)$ Å	U	0	0	0	0.00474(19)
$c = 7.4231(7)$ Å	Rh	1	0	0.5	0.0059(4)
	In(1)	0.5	0	0.30179(11)	0.0078(2)
	In(2)	0.5	0.5	0	0.0076(3)

The magnitude of the phonon contribution to the specific heat for both ternary compounds was determined from a $C/T = \gamma + \beta T^2$ fit to the data (fit interval 1 K < *T* < 10 K). For the U_2RhIn_8 compound, the value of Sommerfeld coefficient yields $\gamma = 47$ mJ mol^{-1} U K^{-2} and the β coefficient equals 3.4 mJ mol^{-1} K^{-4} which corresponds to a Debye temperature $T_D = 150$ K. The Sommerfeld coefficient of $URhIn_5$ equals 60.7 mJ mol^{-1} U K^{-2} while the β coefficient yields the value of 3.3 mJ mol^{-1} K^{-4} corresponding to the Debye temperature of 165 K. The values for $URhIn_5$ are close to those presented recently [24].

Fig. 1(b) represents data in an applied magnetic field of 9 T for U_2RhIn_8 along the [001] axis. The direct comparison with the zero field measurement reveals that T_N is almost unaffected within experimental uncertainty. Equivalent behavior is observed, Fig. 1 (c), in the case of $URhIn_5$. Similar response to magnetic field is observed in the structurally related Ce-based compound, $CeRhIn_5$, where the transition temperature T_N tends to be rather insensitive to the application of magnetic field along the same direction [25].

Fig. 2 shows the temperature dependence of the $\chi(T)$ and $1/\chi(T)$ of U_2RhIn_8 and $URhIn_5$ in magnetic field oriented along [100] and [001] directions and [110] and [001] in the case of UIn_3. The analysis of the $\chi(T)$ data leads to the determination of Néel temperatures as proposed by Fisher [20]; the maximum of the $\partial(\chi(T))/\partial T$ curve. The behavior of the susceptibility curves resembles the one shown for $URhIn_5$ and UIn_3 [19,5], therefore we conclude that the phase transition drives the compound into an antiferromagnetic state. The magnetic susceptibility increases in all compounds with decreasing temperature and this increase is much pronounced for the [001] direction in the ternary compounds. The maximum value of susceptibility is reached at $T_{\chi max} = 130$ K for UIn_3 (consistently with the literature [5]), at $T_{\chi max} = 160$ K for $URhIn_5$ [24] and at $T_{\chi max} = 150$ K for U_2RhIn_8. Such behavior was previously observed in several different uranium compounds [21] and it is generally supposed that this character of the susceptibility curves is associated with antiferromagnetic correlations when approaching T_N. The value of $T_{\chi max}$ for both studied ternary compounds is the highest among uranium compounds up to our knowledge (UPd_2Al_3: $T_{\chi max} = 30$ K; URu_2Si_2: $T_{\chi max} = 60$ K [22]).

In the vicinity of $T_N = 117$ K (98 K, 88 K) for U_2RhIn_8 ($URhIn_5$, UIn_3), a sharp drop of the magnetic susceptibility is observed in agreement with the literature [5,24,19]. This rapid decrease is again more pronounced in the [001] direction in the studied ternary compounds, pointing to the fact that the magnetic moments probably lie in this direction in the ordered state.

At low temperatures ($T \sim 40$ K) the susceptibility reaches its minimum value and rises up again. This increase is negligible in the case of $URhIn_5$ and U_2RhIn_8; however, it plays a dominant role

UNCORRECTED PROOF

Please cite this article as: A. Bartha, et al., Journal of Magnetism and Magnetic Materials (2015), http://dx.doi.org/10.1016/j.jmmm.2015.01.015

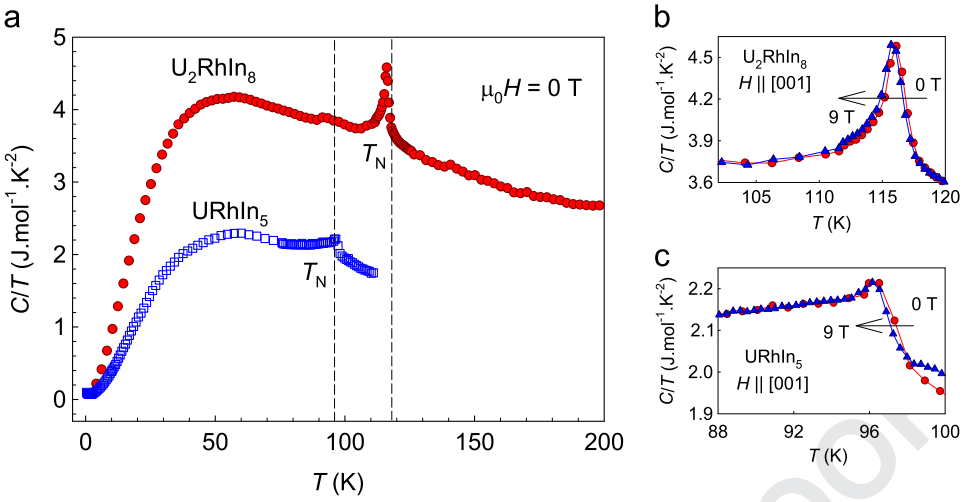


Fig. 1. Temperature dependence of the specific heat divided by temperature (a). The transition into the magnetically ordered state at T_N = 117 K (T_N = 98 K) for U_2RhIn_8 ($URhIn_5$) is marked by vertical dashed lines. Comparison of C/T for U_2RhIn_8 (b) and $URhIn_5$ (c) in zero and 9 T magnetic field applied along the [001] axis.

in case of UIn_3. Previous studies of UIn_3 [5] revealed similar behavior to that presented for ternary compounds. This effect may have intrinsic nature or it could be also connected with a non-negligible amount of paramagnetic impurities, requiring further investigations.

From the character of the $1/\chi(T)$ curves above the Néel temperature it is evident that the behavior of ternary compounds does not follow the Curie–Weiss law in $H \parallel [100]$ direction due to magnetocrystalline anisotropy. The linear behavior appears probably above 400 K, as it is shown i.e. for UPtGa$_5$ [22], which we were able to confirm experimentally in the case of U_2RhIn_8 (see Fig. 2 (a)). Such a recovery of Curie–Weiss law at high temperatures indicates a localized nature of 5*f* electrons. Thus, a crossover of the 5*f* electrons from a low-temperature itinerant nature to a high-temperature localized one is observed. This crossover effect is characteristic for many heavy fermion compounds such as UPt_3, UPd_2Al_3 and URu_2Si_2 [22].

In accordance with previous arguments, we applied the Curie–Weiss law in the $H \parallel [001]$ direction for U_2RhIn_8 and $URhIn_5$, and in [001] and [110] directions in the case of UIn_3. We obtained qualitative values of the effective magnetic moments, summarized in Table 2, that we were able to compare with those previously obtained [24,19,5].The large negative values of paramagnetic Curie temperatures reflect the huge uniaxial magnetocrystalline anisotropy in U_2RhIn_8 and $URhIn_5$ induced by anisotropic 5*f*-ligand hybridization.

The magnetic field dependence of magnetization (see Fig. 3) of U_2RhIn_8 was measured at T=4 K for magnetic field oriented along the [001] and [100] directions. Both magnetization curves reveal linear character up to 7 T; the [100] axis is almost twice higher than the magnetization in the other direction, which resembles the behavior of its more 2D counterpart [24,19]. Using a relation $k_B T_{\chi max} \simeq \mu_B H_c$ [21], where $T_{\chi max}$ = 150 K defines the position of the maximum of the magnetic susceptibility data, and H_c is the critical magnetic field of metamagnetic transition, we obtain a value of H_c = 220 T for U_2RhIn_8. This extremely large value explains the absence of metamagnetic transition in our experimental data.

Fig. 4(a) shows the temperature dependence of the electrical resistivity of U_2RhIn_8 for electrical current *j* applied along the [100] and [110] axes. The room temperature resistivity equals 320 μΩ cm along the [100] direction and is only slightly lower for the [110] direction (310 μΩ cm). The residual resistivity ratio (RRR) exceeds 500 being a sign of a sample of very high quality. The electrical resistivity shows a monotonous decrease down to the value of the transition temperature T_N. Near the transition temperature T_N = 117 K, a tiny kink is observed, accompanied by a second-order phase transition and a formation of a gap at the Fermi surface. Subsequently, the resistivity decreases rapidly with decreasing temperature. The low-temperature part of the electrical resistivity ($2\ K < T_{fit} < 30\ K$) can be fitted well using the equation appropriate for an energy gap (Δ) antiferromagnet with an additional Fermi-liquid term, being $\rho(T) = \rho_0 + AT^2 + DT(1 + 2T/\Delta)\exp(-\Delta/T)$ [26]. Optimal fitting of $\rho^{[100]}$ gives a residual resistivity value ρ_0 = 0.56 μΩ cm, an electron–electron scattering coefficient of A = 0.006 μΩ cm K^{-2}, an electron–magnon and spin-disorder scattering prefactor D = 1.1 μΩ cm K^{-1} and Δ = 118 K. Our fit yielded similar values of the parameters for current applied along the [110] direction.

Fig. 4(b) summarizes the overall temperature dependence of the electrical resistivity of $URhIn_5$ for electrical current *j* applied along the [100], [110] and [001] axes. The room temperature resistivity equals 180 μΩ cm in the basal plane and is only slightly lower for the [001]-axis direction: $\rho^{[001]}$ = 170 μΩ cm. Note that $\rho^{[100]}$ (300 K) is almost the same as reported by Matsumoto and coworkers [24]. Similar to U_2RhIn_8, the RRR ~200 of the $URhIn_5$ single crystals confirms their high quality. The data manifest distinct anomalies with onset at around T ~100 K for $\rho^{[001]}$ and at a slightly lower temperature T=98 K for $\rho^{[100]}$ and $\rho^{[110]}$ which is reminiscent of the Néel temperature anomaly for $\rho(T)$ in pure Cr [31] – a spin-density-wave (SDW) antiferromagnet. Accordingly, the onset marks T_N and the increase in resistivity result from opening of the SDW gap. Below T_N, the resistivity drops down rapidly in all directions. The low-temperature part was fitted according to similar formula as for U_2RhIn_8 with results ρ_0 = 1 μΩ cm, A = 0.013 μΩ cm K^{-2}, D = 0.35 μΩ cm K^{-1} and Δ = 82 K. Our fit yielded similar values of the parameters for current along the [110] direction. However, in the case of $j \parallel [001]$ we obtained a somewhat higher value of the gap energy Δ = 119 K.

After evaluating the data from specific heat and electrical resistivity measurements of U_2RhIn_8 and $URhIn_5$, the Kadowaki–Woods [27] ratio A/γ^2 could be calculated, where A is the coefficient of the quadratic term in the temperature dependence of electrical resistivity. The value of 2×10^{-6} μΩ cm (mol K/mJ)^2 for U_2RhIn_8 and 3.6 10^{-6} μΩcm (mol K/mJ)^2 for $URhIn_5$ was obtained, being one order of magnitude lower than in the common heavy-fermion systems [28].

To investigate the effect of hydrostatic pressure, we performed electrical resistivity measurement of U_2RhIn_8 up to 3.2 GPa. The

UNCORRECTED PROOF

Please cite this article as: A. Bartha, et al., Journal of Magnetism and Magnetic Materials (2015), http://dx.doi.org/10.1016/j.jmmm.2015.01.015

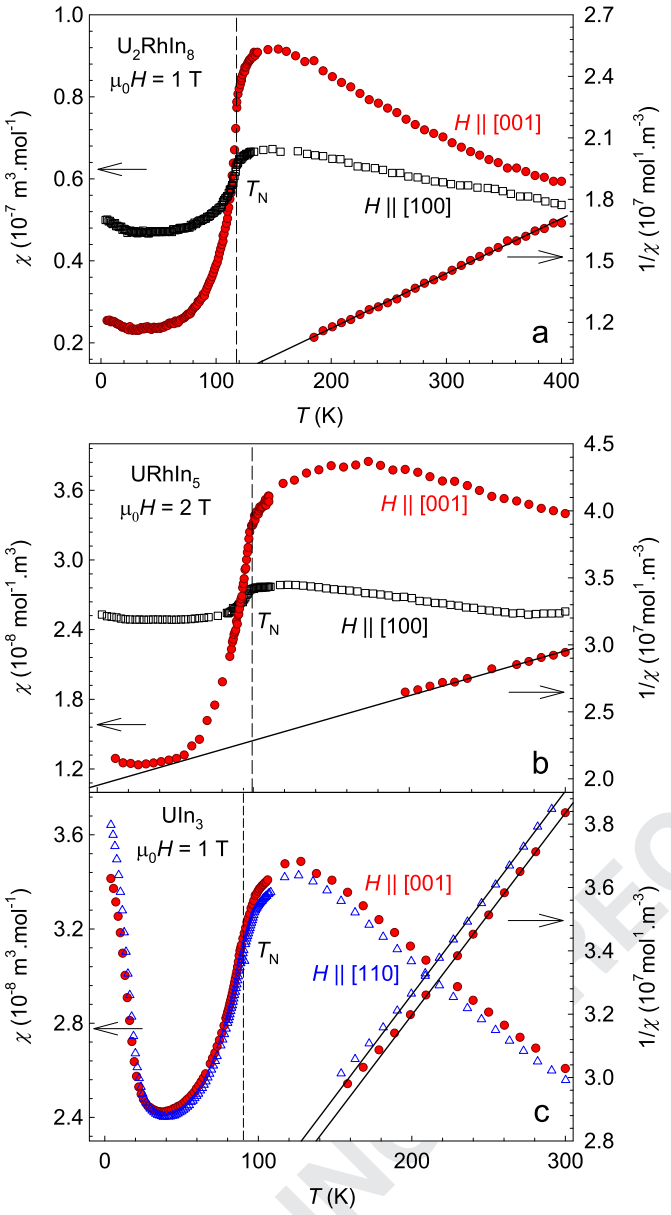


Fig. 2. Temperature dependence of $\chi(T)$ and $1/\chi(T)$ and Curie–Weiss fit of (a) U_2RhIn_8, (b) $URhIn_5$ and (c) UIn_3 for magnetic field oriented along the [100] and [001] directions in the case of U_2RhIn_8 and $URhIn_5$, along the [100] and [110] direction for UIn_3. Vertical dashed line marks the transition temperature T_N.

Table 2
Néel temperatures, effective magnetic moments obtained from Curie–Weiss fits and paramagnetic Curie temperatures for different orientations of magnetic fields for UIn_3 ([001] and [110] orientations), U_2RhIn_8 and $URhIn_5$.

	UIn_3	U_2RhIn_8	$URhIn_5$
***H*|| [001]**			
T_N (K)	88	117	98
μ_{eff} (μ_B/U)	3.16	3.45	3.6
θ_p(K)	−300	−240	−400
***H*|| [110]**			
μ_{eff} (μ_B/U)	3.15	–	–
θ_p (K)	−310	–	–

Néel temperature increases gradually with hydrostatic pressure, as is shown in the T–p phase diagram in Fig. 5. A possible explanation of the positive pressure dependence of T_N is given by the spin-

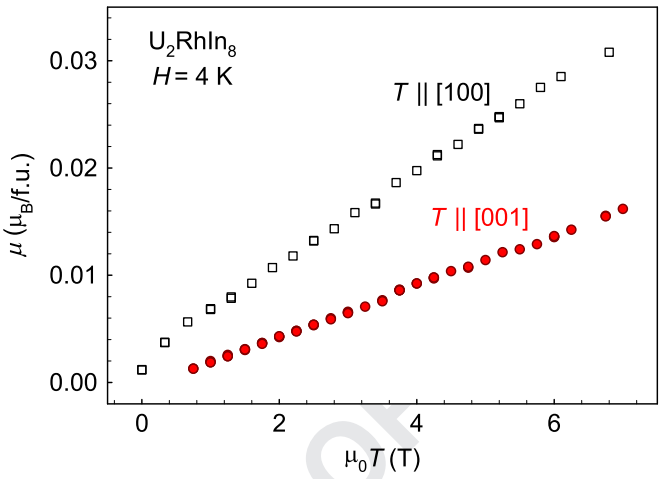


Fig. 3. Magnetic field dependence of magnetization taken at 4 K of U_2RhIn_8 in magnetic field oriented along the [100] and [001] axes.

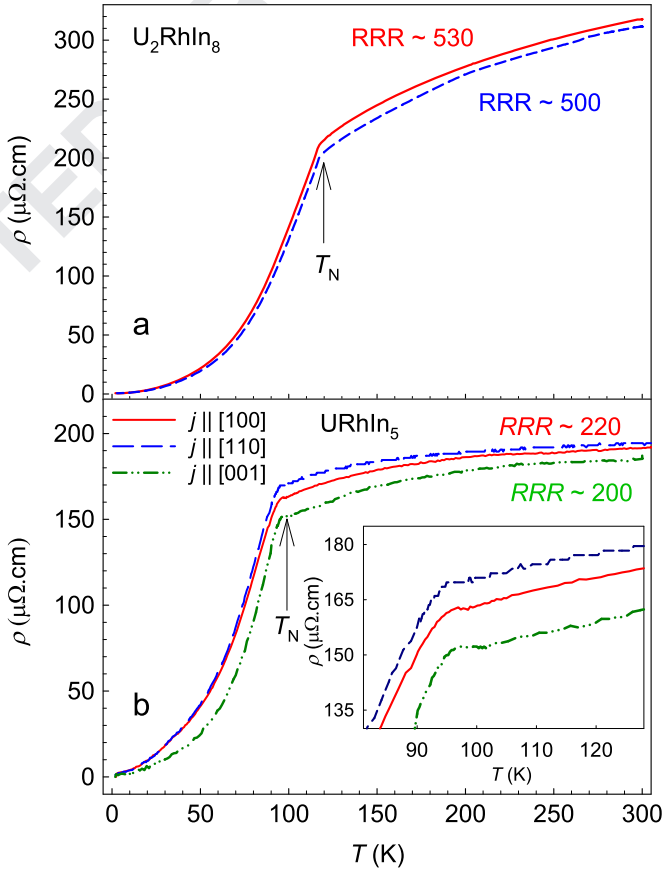


Fig. 4. Temperature dependence of the electrical resistivity for electrical current applied along [100] and [110] directions is shown for U_2RhIn_8 (a). The temperature dependence of the electrical resistivity for current applied along the [100], [110] and [001] directions for $URhIn_5$ compound (b). The inset in Fig. 4(b) shows the transition in detail. The arrows mark the onset of the antiferromagnetic transition at T_N = 117 K (T_N = 98 K) for U_2RhIn_8 ($URhIn_5$). One legend applies for both figures.

fluctuation theory of an itinerant 5*f* electron system alongside with the Hubbard model [29,30]. According to this scenario, hydrostatic pressure induces an increase in the hybridization between 5*f* and conduction electrons, which strengthens the exchange coupling J between U ions. On the other hand, it also decreases the 5*f* magnetic moment at the uranium site. The value of T_N changes from 117 K to 128 K at ambient pressure and 3.2 GPa, respectively, with the rate of 5.4 $\pm$0.9 K GPa^{-1}. This slope

UNCORRECTED PROOF

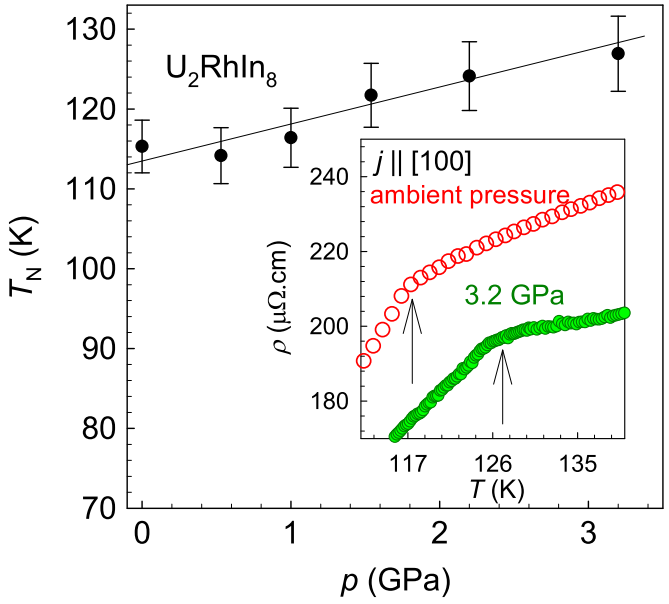


Fig. 5. Temperature–pressure phase diagram of U_2RhIn_8. Inset shows the temperature dependence of the electrical resistivity for electrical current applied along the [100] direction at ambient pressure and at 3.2 GPa. Arrows indicate the transition at T_N.

corresponds well to the pressure evolution of T_N in $URhIn_5$ [24]. The detail of the resistivity curve near T_N for ambient pressure and for 3.2 GPa with electrical current applied along the [001] axis is shown in the inset of Fig. 5.

The ternary compounds U_nTX_{3n+2} with T = Rh and X = In represent a system which offers the possibility to study the effect of structural dimensionality on the magnetism of uranium layered structures. Dimensionality develops from 3D towards 2D when spanning the series: UIn_3 (1–0–3) → U_2RhIn_8 (2–1–8)→ $URhIn_5$ (1–1–5) . In the other cases, either only the cubic compound (USn_3, UPb_3 [32]) or the cubic compound (UGa_3 [33]) together with its 1–1–5 (or 2–1–8) parent system (T = Fe, Co, Ni, Pd, Ir, Pt [34,35,9,36,37]) is known. The Ga-based compounds with T = Fe, Rh, which form both 1–1–5 and 2–1–8 are paramagnetic. Since all the known U_nRhIn_{3n+2} compounds order antiferromagnetically, a T_N vs. c/a diagram can be constructed (see Fig. 6) in order to study the effect of structural dimensionality on the magnetic ordering. The evolution of transition temperature does not follow the dimensionality sequence "1–0–3 → 2–1–8 → 1–1–5" as discussed by Cornelius et al. [25]. In contrast to the behavior in cerium compounds [25], the Néel temperatures of U_nRhIn_{3n+2} reveal a monotonic evolution with respect to the c/a ratio. A possible explanation of this discrepancy is given by the different driving microscopic mechanisms in the compounds. The microscopic mechanisms in Ce-based compounds are mostly RKKY-type while in the uranium compounds the 5f-ligand hybridization plays a substantial role. Moreover, the cerium compounds order magnetically well below 10 K while the ordering temperature in the case of U-based compounds is at least an order of magnitude higher.

The spin-polarized LSDA calculation splits the spin-up and spin-down bands with spin magnetic moment at uranium site 2.17 μ_B. Since strong magnetocrystalline anisotropy is present, the spin–orbit coupling is also included into calculations. The calculated spin magnetic moment at uranium site decreases to $M_S = 1.744\ \mu_B$ and the orbital magnetic moment $M_L = -2.418\ \mu_B$ is antiparallel. Magnetic moments located at rhodium and indium sites are both smaller than 0.1 μ_B. Total uranium magnetic moment is $|M_T| = 0.674\ \mu_B$. From comparison with $URhIn_5$ we expected larger total uranium moment about $|M_T| = 1.6\ \mu_B$. Thus, the

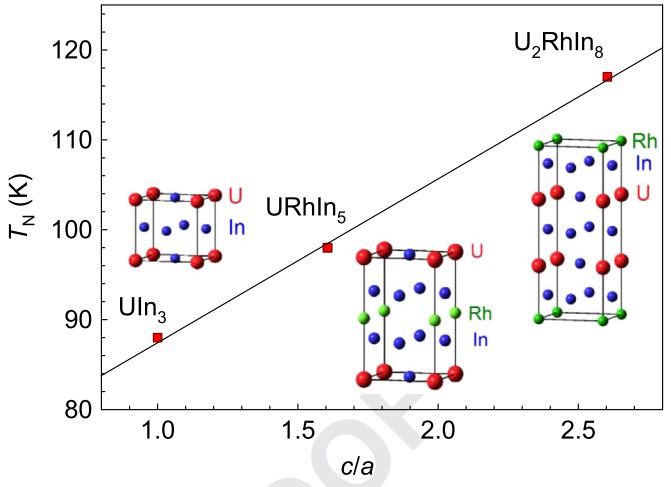


Fig. 6. T_N vs. c/a diagram depicting the relation of the structural dimensionality and magnetism of uranium layered structures. The points are accompanied by the structures of UIn_3 (cubic), $URhIn_5$ (tetragonal) and U_2RhIn_8 (tetragonal) compounds. Solid black line is a guide to the eye.

correlation movement of 5f electrons is not negligible. Therefore we used LSDA+U method to describe correlated movement of 5f electrons. Tuning effective Hubbard U we have found spin magnetic moment $M_S = 1.738\ \mu_B$ and orbital magnetic moment $M_L = -3.3\ \mu_B$ providing the total magnetic moment $|M_T| = 1.592\ \mu_B$ for medium effective U=1.3 eV. We are fully aware that such calculation loses its first-principle character on this level, but on the other hand, we showed that these heuristically derived values of effective U allow us to obtain valuable results.

4. Conclusions

Single crystals of UIn_3, $URhIn_5$ and the novel U_2RhIn_8 phase were synthesized using the In self-flux method and studied by means of magnetization, thermodynamic and transport measurements. The U_2RhIn_8 compound adopts the Ho_2CoGa_8-type structure with lattice parameters a=4.6056(6) Å and c=11.9911(15) Å. Measurements of specific heat and magnetization revealed a second-order phase transition into the antiferromagnetic state at T_N = 117 K. The compounds UIn_3 and $URhIn_5$ order antiferromagnetically below T_N = 88 K and 98 K, respectively, in accordance with the literature [5,24]. Electrical resistivity measurement revealed the very high quality of the studied ternary compounds with RRR exceeding 200 and 500, respectively. The temperature dependence of magnetic susceptibility for $URhIn_5$ and U_2RhIn_8 reveals strong magnetic anisotropy and suggests that both systems undergo an itinerant-localized crossover at high temperatures above 300 K, similar to other uranium-based compounds (UPd_2Al_3, URu_2Si_2 [22]), including $UPtGa_5$ [22] from the same group of compounds. The application of hydrostatic pressure supports the robustness of the antiferromagnetic phase in both ternary compounds with similar pressure coefficients [24]. Successful synthesis of U_2RhIn_8 provides an opportunity among 5f systems to study the evolution of ground state properties depending on c/a ratio. As is shown in Fig. 6 the evolution of T_N is monotonic with respect to c/a ratio. This behavior is in contrast with the cerium analogs [25] and will be a subject of further investigation.

Uncited references

[12,23]. Q2

UNCORRECTED PROOF

ARTICLE IN PRESS

Acknowledgment

Experiments were performed in MLTL (http://mltl.eu/), which is supported within the program of Czech Research Infrastructures (Project no. LM2011025). Our work was supported by the Grant Agency of the Charles University (Project no. 362214) and Czech Science Foundation (Project P203/12/1201). Single crystal *X*-ray diffraction was performed in the Department of Structure Analysis, Institute of Physics ASCR.

References

[1] H.H. Hill, Plutonium 1970 and Other Actinides, AIME, New York, 1970, p. 2.
[2] Y. Tokiwa, H. Harima, D. Aoki, S. Nojiri, M. Murakawa, K. Miyake, N. Watanabe, R. Settai, Y. Inada, H. Sugawara, H. Sato, Y. Haga, E. Yamamoto, Y. Ōnuki, J. Phys. Soc. Jpn. 69 (2000) 1105–1112.
[3] G.W. Crabtree, B.D. Dunlap, D.D. Koelling, Physica B 135 (1985) 38–40.
[4] A. Hasegawa, J. Phys. Soc. Jpn. 53 (1984) 3929–3937.
[5] Y. Tokiwa, D. Aoki, Y. Haga, E. Yamamoto, S. Ikeda, R. Settai, A. Nakamura, Y. Ōnuki, J. Phys. Soc. Jpn. 70 (2001) 3326–3330.
[6] A. Murasik, P. Fischer, Z. Zolnierek, Physica B 102 (1980) 188–191.
[7] S. Ikeda, T. Ōkubo, Y. Inada, Y. Tokiwa, K. Kaneko, T.D. Matsuda, E. Yamamoto, Y. Haga, Y. Ōnuki, J. Phys.: Condens. Matter 15 (2003) S2015–S2018.
[8] M. Schönert, S. Corsépius, E.W. Scheidt, G.R. Stewart, J. Alloys Compd. 224 (1995) 108–110.
[9] V. Sechovský, L. Havela, G. Schaudy, G. Hilscher, N. Pillmayr, P. Rogl, P. Fischer, J. Magn. Magn. Mater. 104–107 (1992) 11–12.
[10] C. Pfleiderer, Rev. Mod. Phys. 81 (2009) 1551.
[11] Y. Haga, T. Honma, E. Yamamoto, H. Ohkuni, Y. Onuki, M. Ito, N. Kimura, J. Jpn. Appl. 37 (1998) 3604.
[12] J. Custers, K.-A. Lorenzer, M. Müller, A. Prokofiev, A. Sidorenko, H. Winkler, A. M. Strydom, Y. Shimura, T. Sakakibara, R. Yu, Q. Si, S. Paschen, Nat. Mat. 11 (2012) 189–194.
[13] L. Palatinus, G. Chapuis, J. Appl. Crystallogr. 40 (2007) 786–790.
[14] V. Petricek, M. Dusek, L. Palatinus, Z. Kristallogr. 229 (5) (2014) 345–352.
[15] N. Fujiwara, T. Matsumoto, K. Koyama-Nakazawa, A. Hisada, Y. Uwatoko, Rev. Sci. Instrum. 78 (2007) 073905.
[16] K. Murata, H. Yoshino, H.O. Yudav, Y. Honda, N. Shirakawa, Rev. Sci. Instrum. 68 (1997) 2490.
[17] K. Schwarz, P. Blaha, G. Madsen, Comput. Phys. Commun. 147 (2002) 71.
[18] J. Kunes, P. Novak, M. Divis, P.M. Oppeneer, Phys. Rev. B 63 (2001) 205111.
[19] A. Bartha, M. Kratochvílová, M. Dušek, V. Sechovský, J. Custers, Acta Phys. Polon. A (2015), in press. Q3
[20] M.E. Fisher, Philos. Mag. 7(82) (1962) 1731.
[21] N. Tateiwa, S. Ikeda, Y. Haga, T.D. Matsuda, E. Yamamoto, K. Sugiyama, M. Hagiwara, K. Kindo, Y. Ōnuki, J. Phys. Soc. Jpn. 80 (2011) 014706, and references therein.
[22] A. Galatanu, Y. Haga, T.D. Matsuda, S. Ikeda, E. Yamamoto, D. Aoki, T. Takeuchi, Y. Ōnuki, J. Phys. Soc. Jpn. 74 (2005) 1582.
[23] Y. Onuki, A. Hasegawa, in: K.A. Gschneider Jr., L. Eyring (Eds.), Handbook on the Physics and Chemistry of Rare Earths, vol. 20, Elsevier, Amsterdam, 1995, p. 1.
[24] Y. Matsumoto, Y. Haga, N. Tateiwa, H. Sakai, T.D. Matsuda, E. Yamamoto, Z. Fisk, Phys. Rev. B 88 (2013) 045120.
[25] A.L. Cornelius, P.G. Pagliuso, M.F. Hundley, J.L. Sarrao, Phys. Rev. B 64 (2001) 144411.
[26] N.H. Andersen, H. Smith, Phys. Rev. B 19 (1979) 384.
[27] K. Kadowaki, S.B. Woods, Solid State Commun. 58 (1986) 507.
[28] N. Tsuji, H. Kontani, K. Yoshimura, Phys. Rev. Lett. 94 (2005) 057201.
[29] B.R. Cooper, Q.G. Sheng, U. Benedict, P. Link, J. Alloys Compd. 213–214 (1994) 120.
[30] Q.G. Sheng, B.R. Cooper, J. Magn. Magn. Mater. 164 (1996) 335.
[31] O. Rapp, G. Benediktsson, H.U. Astrom, S. Arajs, K.V. Rao, Phys. Rev. B 18 (1978) 3665.
[32] K. Sugiyama, T. Iizuka, D. Aoki, Y. Tokiwa, K. Miyake, N. Watanabe, K. Kindo, T. Inoue, E. Yamamoto, Y. Haga, Y. Ōnuki, J. Phys. Soc. Jpn. 71 (2002) 326–331.
[33] D. Kaczorowski, R. Hauser, A. Czopnik, Physica B 230 (1997) 35–38.
[34] Y. Tokiwa, T. Maehira, S. Ikeda, Y. Haga, E. Yamamoto, A. Nakamura, Y. Ōnuki, M. Higuchi, A. Hasegawa, J. Phys. Soc. Jpn. 70 (2001) 2982–2988.
[35] R. Wawryk, Z. Henkie, T. Cichorek, C. Geibel, F. Steglich, Phys. Status Solidi B 232 (2002) R4–R6.
[36] Y. Tokiwa, S. Ikeda, Y. Haga, T. Okubo, T. Iizuka, K. Sugiyama, A. Nakamura, Y. Ōnuki, J. Phys. Soc. Jpn. 71 (2002) 845–851.
[37] S. Ikeda, T. Ōkubo, Y. Inada, Y. Tokiwa, K. Kaneko, T.D. Matsuda, E. Yamamoto, Y. Haga, Y. Ōnuki, J. Phys.: Condens. Matter 15 (2003) S2015–S2018.

UNCORRECTED PROOF

Please cite this article as: A. Bartha, et al., Journal of Magnetism and Magnetic Materials (2015), http://dx.doi.org/10.1016/j.jmmm.2015.01.015